Ab initio based interface modeling for fully coherent precipitates of arbitrary size in Al alloys

Flemming J. H. Ehlers* and Randi Holmestad
Dept. of Physics, Norwegian University of Science and Technology (NTNU), 7491 Trondheim, Norway

* Corresponding Author: Flemming J. H. Ehlers
Dept. of Physics, Norwegian University for Science and Technology NTNU, 7491 Trondheim, Norway
email: flemming.ehlers@ntnu.no
Tel: +47 7359 3480; Fax: +47 7359 7710

Abstract

An *ab initio* based atomistic model scheme for an approximate determination of the interfacial and strain energies for the entire interface of a fully coherent precipitate in a host lattice is presented. For each given presumed compositionally abrupt interface, the model incorporates the effect of the strain evolution along the interface by use of a sequence of supercells. Each cell in this sequence has been distorted to describe the local interface region in question with the optimal accuracy allowed by periodic boundary conditions. Together, the cells comprise a shell of nm thickness, enclosing the full interface and its strongly affected near vicinity. The computational demands for the scheme are connected with the number of atoms in a given interface region cell, i.e., no scaling with precipitate size occurs – other than the number of cells required. In practice, this allows performing calculations for essentially all precipitate sizes. The scheme has been tested for the case of the main hardening precipitate β" in the Al–Mg–Si alloy system and compared quantitatively with presently available alternatives. Implementation in an atomic hybrid model scheme for a full description of the precipitate interface energy should be realistic.

Keywords: First-principles calculations, Aluminum alloys, Precipitate-host lattice interfaces, Interface energies

1. Introduction

The main hardening precipitates of a given age hardenable Al alloy system are generally

characterized by a high level of coherency with the host lattice [1], with negligible subsystem misfit along at least one direction, but significant misfit (and sometimes even breakdown of coherency) along remaining basis vector directions. These properties largely explain [2] the early appearance of such phases in the precipitation sequence as well as the strongly limited individual precipitate sizes and high number densities – qualities instrumental in impeding the motion of dislocations, leading to materials hardening [3].

It is well established [4,5] that any theoretical optimization of an age hardenable Al alloy requires as its input precipitate-host lattice interfacial and strain energies for a reliable prediction of the microstructure and its effect on materials properties. Moreover, it follows from the above described properties of the main hardening precipitates of key interest, that a theoretical determination of such energies will likely require *ab initio* based studies of close to the *entire* precipitate-host lattice interface. Firstly, close to the interface, a linear elasticity theory (LET) based description of the individual subsystems breaks down as it fails to take into account the electronic effects of the interacting subsystems, i.e. the interfacial energy. Secondly, *along* a high misfit direction on a coherent interface, an additional problem arises from the significant strain evolution present – once again a task beyond the full capability of LET.

Over the last decade in particular, transmission electron microscopy (TEM) based studies have structurally clarified a considerable amount of the precipitates encountered for the various Al alloy sequences (see e.g. [6-8]). Nonetheless, experimental analysis of the main hardening precipitate interface energies is generally highly complicated – if not entirely out of reach – due to the metastable nature of the phases involved. Theoretical studies in turn are presently hampered by the significant limitation on the number of atoms in the model system, as compared to the typical number connected with a physically sized and well isolated precipitate in host lattice surroundings. Currently, *ab initio* model based determinations of interfacial and strain energies focus on *single local regions* for each interface with different orientation (see e.g. [5,9]), leaving considerations on the strain evolution effects to LET. As stressed above, the accuracy of such an approach is questionable when dealing with coherent interfaces with high misfit.

The present work focuses on the situation of a fully coherent precipitate with compositionally abrupt interfaces. For this general group of precipitates, we show that it is possible to model

essentially the full interface (with interpolation needed for the precipitate edges) – within an *ab initio* based framework and at the precision normally deemed acceptable for the local regions probed in e.g. [9]. For each interface under consideration, our scheme employs a *sequence* of precipitate-host lattice supercells, differing in their level of basis vector distortions relative to a fully optimized geometry. We stress that if these cell distortions are chosen to correlate with the strain evolution along the various directions on the interface, the resulting patchwork of cells will always describe the local interface properties at the optimal precision achievable. As each supercell in this patchwork is probed individually, the model scheme represents an $O(N)$ problem, where the number of atoms in each cell N is typically only a few tens of atoms. This indicates a tremendous computational simplification when compared to optimizing the full precipitate-host lattice system with *ab initio* based methods: basically, the precipitate size is no longer a limiting factor.

The paper is managed as follows: in Sec. 2, we clarify the ideas behind the model scheme. The basic equations underlying this scheme are presented in Sec. 3, with direct comparison made to currently available *ab initio* based alternatives. Sec. 4 introduces the selected precipitate for the test simulations, the main hardening β" phase of the Al–Mg–Si alloy system, along with a presentation of computational details. The results of the calculations are described in Sec. 5: here, the new model scheme of this work is compared to a conventional scheme where the strain energy evolution is determined with LET. Sec. 6 summarizes our main findings, while key output energies are tabulated in App. A.

2. Basic ideas behind the model scheme

2.1. Preliminary remarks

It is presently not realistic to model, within an *ab initio* based framework, a physically sized system of a precipitate enclosed in a host lattice. For a needle shaped precipitate, it might be defended to use a slab geometry (Fig. 1a), surrounding this phase with host atoms in the cross section plane only and assuming a formally infinite precipitate along the main growth direction. While this modeling approach greatly reduces the number of atoms in the system, the requirements for physical precipitate cross section dimensions and acceptable precipitate separation in the supercell based model scheme still generally necessitate the incorporation of a thousand atoms or more in the system. With current computational resources, this is a rather prohibitive number.

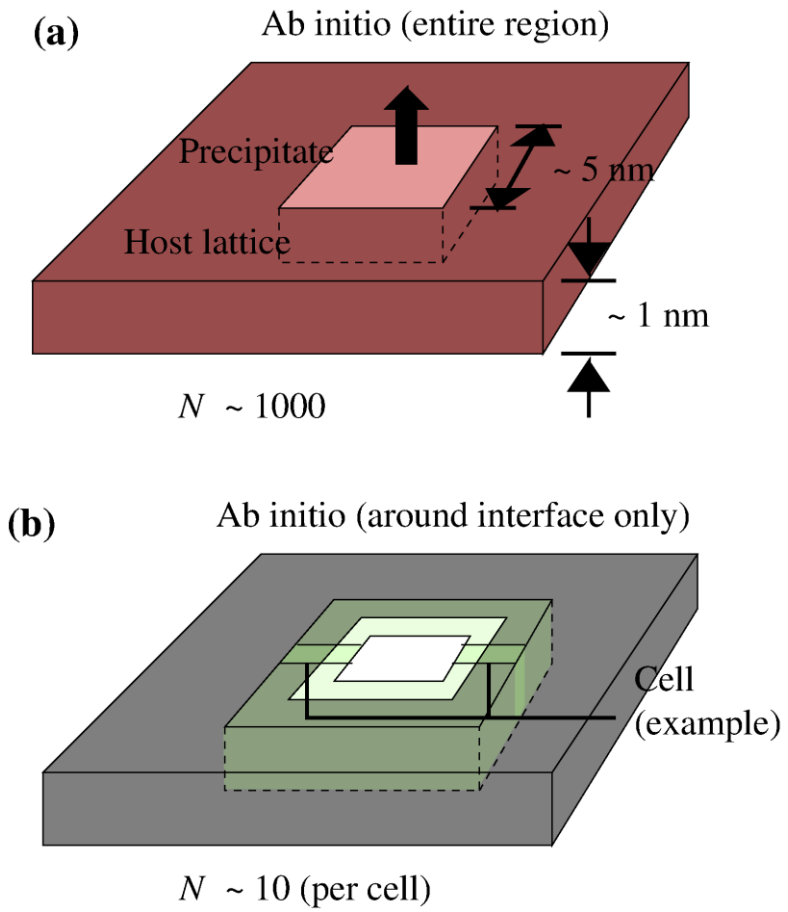

Fig. 1. (a) Schematic presentation of a fully coherent needle shaped precipitate, as described with a slab geometry which assumes a formally infinite precipitate along the main growth direction (single black arrow). For a physically sized and well isolated precipitate, this slab will generally contain beyond a thousand atoms, making *ab initio* based calculations impractical. (b) Suggested model scheme of the present work: Only a thin (≈ nm width) region enclosing the precipitate-host lattice interface of (a) is modeled with *ab initio* methods, using a sequence of supercells distorted according to the position on the interface. Each cell (example highlighted) contains only a few tens of atoms and is easily tractable, regardless of precipitate size.

Up to now, the choice in *ab initio* based interface model schemes has been to focus on local regions on the interface – a single interface region supercell like the one highlighted in Fig. 1b has been employed for describing the properties of the whole interface of the given orientation (see e.g. [9]). In Sec. 2.2, 2.3 we shall clarify, firstly, why such a cell size limitation must seem necessary when the interface under investigation is coherent with significant subsystem misfit. Secondly, we shall argue how optimal accuracy within this model framework is to be expected only for a local region

(as opposed to the full interface of this orientation), of the same extension as the supercell. Building upon this argument (Sec. 2.4), leads directly to the general idea behind the model scheme of this work, where a sequence of different supercells together enclose the entire interface as in Fig. 1b.

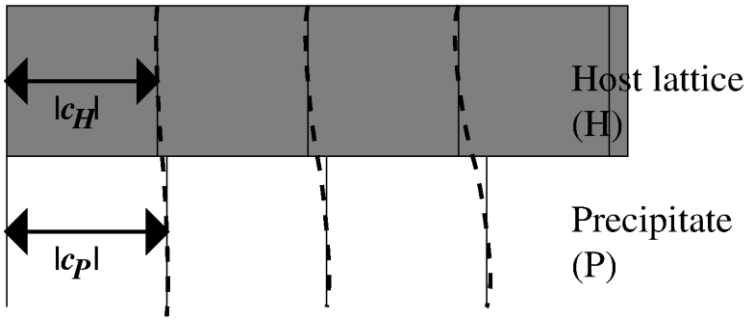

Fig. 2. Schematic illustration of a coherent interface with significant misfit between the subsystems. The straight horizontal line at the figure center describes the interface while the straight vertical lines above (below) this line highlight the periodicity $|\boldsymbol{c}_H|$ ($|\boldsymbol{c}_P|$) for the bulk host lattice (precipitate) along the interface. The broad dashed lines highlight the distortions around the interface arising from the subsystem interactions.

2.2. A coherent interface with significant subsystem misfit

Fig. 2 shows a schematic presentation of a coherent interface between two subsystems with significant misfit along one direction ($\boldsymbol{c}_H$) in the interface plane. In the context of the present discussion, this system should be viewed as representing an area of a selected interface of Fig. 1b, away from the precipitate corners. As a consequence of the interaction between the two subsystems, both are distorted to some extent in the vicinity of the interface. This strain increases along the interface in response to the accumulated misfit between the subsystems. In Fig. 2, the point of minimal strain at the interface is located at the left side of the figure. For the case of a precipitate in a host lattice, misfit elimination generally is not encountered, as it would require the precipitate to match the fully surrounding host. With $|\boldsymbol{c}_P| > |\boldsymbol{c}_H|$ as shown in Fig. 2, the precipitate-host lattice misfit $m_{\boldsymbol{c}} = (|\boldsymbol{c}_P| - |\boldsymbol{c}_H|)/|\boldsymbol{c}_H|$ is defined as positive.

2.3. Limitations to a supercell based model description

It is evident that the strain along the interface in Fig. 2 will increase continuously when moving from left to right. From a model perspective, this fact poses a fundamental challenge whenever the theoretical framework used (supercell formalism) involves periodic boundary

conditions (PBCs). As the PBC itself dictates a repetition of the system, a whole strain evolution cycle must be described *within* the model system for full compatibility with the physical case of Fig. 2. Below, we shall discuss the key reason why this requirement is unlikely to be met for a coherent precipitate-host lattice interface with significant subsystem misfit in a practical *ab initio* based calculation.

In principle, the value of $|\boldsymbol{c}_P|/|\boldsymbol{c}_H|$ for the system in Fig. 2 can always be viewed as being well approximated by some ratio m/n of two integer numbers m, n. From this perspective, modeling the whole strain evolution cycle along the interface will simply require a supercell containing m (n) host lattice (precipitate) unit cells along the interface, as $n|\boldsymbol{c}_P| \approx m|\boldsymbol{c}_H|$. In a first principles based study, however, both m and n will have to be quite small due to the severe limitation on the number of atoms in the model system. Unless $m \approx n$ (implying negligible misfit in Fig. 2), the requirement for small integers m, n almost certainly leads to $m_{\mathbf{c}}$ exceeding the maximum value (little more than 5%) associated with a coherent interface. In other words, only semicoherent interfaces can actually be described. While not unphysical, such interfaces are clearly less frequently encountered for the main hardening precipitates of an alloy, making the limitation highly restrictive.

It emerges that for coherent interfaces with significant misfit, model approximations will necessarily have to be made – as argued above, the physical misfit does not allow for an accurate description. The conventionally chosen alternative [5,9] is to formally assume $m_{\mathbf{c}} = 0$, i.e., to adopt the approximation of mutually fully adapting subsystems in the interface plane [10]. This leads to an easily tractable (minimal possible size) interface model system – but the physical strain evolution occurring along the interface within the boundaries of this supercell is always truncated by the PBCs in this model description.

2.4. Introduction to the present modeling scheme

As discussed in Sec. 2.3, the coherent precipitate-host lattice interface with significant misfit in practice will have to be modeled sequentially in an *ab initio* based study, with only small segments of the complete interface described by a given supercell in the sequence. Fig. 3a describes the way this problem is normally attacked: around the point of minimal strain (middle of the figure), the cell to be used for the description of the physical system is straightforwardly obtained by fully optimizing the structural parameters and cell dimensions. This minimizes the strain for the model

system, resulting in the optimal description of the physical region. However, normally, the same cell is used for describing all other segments of the interface as well. Since strain evolution is truncated within each supercell, the use of identical supercells throughout has the consequence that the *whole* strain evolution along the interface – the progression from straight to bending vertical lines in Fig. 3 (a) – is effectively neglected. This will necessarily lead to a quite erroneous determination of the interface energy. Further, given the appreciable values for the accumulated strain at the physical interface, the omitted stress contributions in the modeling are unlikely to be precisely described by a LET based scheme in a separate analysis.

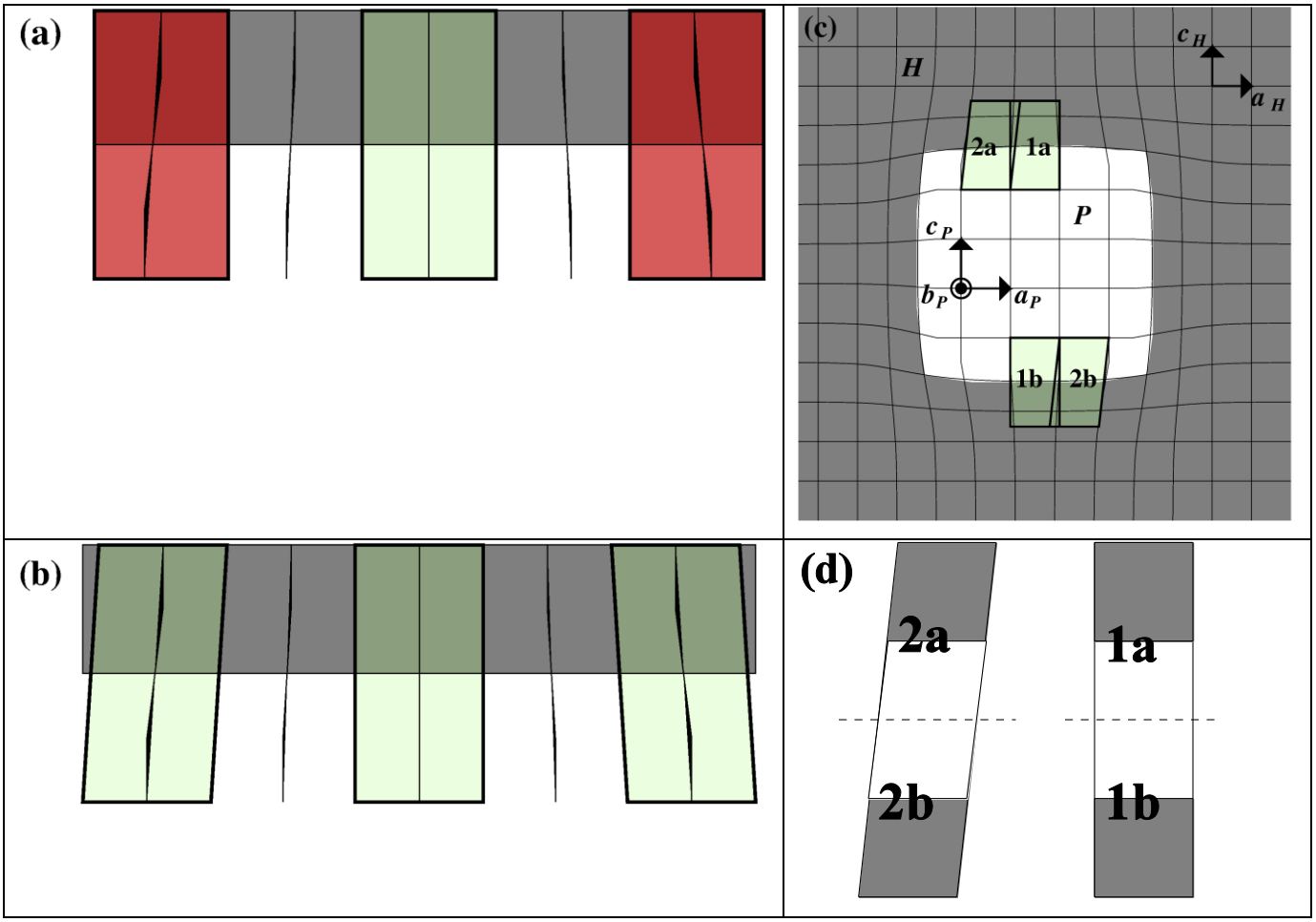

Fig. 3. (a) Schematic illustration of a coherent interface with significant misfit between the subsystems. In comparison with Fig. 2, the point of minimal strain is now located in the middle of the figure, and only the broad dashed lines from that figure are now highlighted (as full lines). The central light green box denotes the part of the unit cell describing the region of minimal strain on this interface. This cell ceases to provide an optimal (within the model limitations) description of the system away from this region (dark red boxes). (b) In the model scheme of this work, each local

region on the interface is described with a supercell distorted to match the local strain for the physical system. Compared to (a), optimal accuracy is now achieved for the whole interface. (c) Schematic illustration of the full precipitate-host lattice system and the construction scheme for the general interface region cell (compare with Fig. 1b). As shown in this figure, symmetrically equivalent regions on each side of the precipitate are always coupled, with the numbers emphasizing connected cell halves. (d) The supercells emerging from (c), viewed in isolation.

The model scheme presented in this work takes on a different path: as shown in Fig. 3b, the cell used for describing the region of minimal strain remains the same as in Fig. 3a, but away from this segment, the supercell is distorted according to the strain evolution for the physical system. If these cell distortions are chosen to match the actual distortions present in the center of the region covered by the cell, this new model scheme will retain the precision along the interface.

As indicated in Fig. 1b already, Fig. 3a, 3b only display halves of the full supercells – the PBCs require the presence of two interfaces within the system. As shown in Fig. 3c, all required cells can be constructed straightforwardly by combining symmetrically equivalent regions on each side of the full precipitate, leading to the cells of Fig. 3d. It should hence be possible to describe the whole interior of each precipitate-host lattice interface (interpolating the corners) by suitable choices of supercell distortions.

3. Model scheme equations

3.1. System under consideration

At zero temperature, the formation enthalpy $\Delta H_{\mathrm{P}}^{SS}$ of a stoichiometric precipitate 'P' in a host lattice as defined relative to the component atoms in a supersaturated solid solution (SS) can generally be obtained as:

$$\Delta H_{\mathrm{P}}^{SS} = (1/N_{\mathrm{P}})\{N_{\mathrm{P}}\Delta H_{\mathrm{P,\,Bulk}}^{SS} + \zeta N_{\mathrm{PH}}^{\zeta} + \sigma A_{\mathrm{P}}\}. \qquad (1)$$

In this expression, the first term on the right hand side denotes the approximate formation enthalpy $\Delta H_{\mathrm{P,\,Bulk}}^{SS}$ as obtained when ignoring precipitate-host lattice interactions (hence the additional subscript 'Bulk'). Here, N_{P} represents the number of atoms contained in the precipitate. This term,

while generally dominant (quite often, see e.g. [11], ΔH_P^{SS} is identified with $\Delta H_{P,\,Bulk}^{SS}$ in calculations), is not of central interest in the present work, as it makes no reference to the subsystem interfaces. The details for its determination are outlined in [11]. The second and third terms in (1) represent the energy penalties associated with the subsystem interactions ignored in the first term: within the region (comprising N_{PH}^{ζ} atoms) where the strain on the two subsystems is deemed non-negligible, the (average) strain energy is given by ζ. The chemical interaction between the subsystems is expressed in the last term as the product of the (average) interfacial energy σ and the precipitate surface area A_P. It is evident that modeling the precipitate-host lattice interactions increasingly well is characterized by the improved accuracy in the parameters σ and ζ.

For simplicity, our focus below is on a fully coherent needle shaped precipitate with significant misfit values in the needle cross section and negligible misfit along the needle direction. Further, we assume compositionally abrupt and defect free precipitate-host lattice interfaces with identical interface configurations for interfaces of the same orientation, and ignore the end points of the needle. Within these approximations, only a slab of precipitate unit cell thickness along the needle direction is needed for describing the full system. Along the other two directions, the slab should be sufficiently large to include all non-negligible strain contributions. A schematic presentation of this system is shown in Fig. 3c. With a system thickness normal to the paper (needle direction) of only one precipitate unit cell width, evidently only part of the precipitate, containing N_P^{Slab} atoms, is rigorously considered. The full precipitate area is now replaced by a ribbon of area A_P^{Slab} at the boundary between the (presumed well defined) white and gray regions.

3.2. Interfacial and strain energy expressions

As discussed in Sec. 2.1, direct modeling of the system in Fig. 3c within an *ab initio* based theoretical framework is not normally feasible. Rather, the approach to determining σ and ζ technically involves modeling the full precipitate-host lattice interface as a 'patchwork' of small local interface regions (see Sec. 2.4). The conventional model scheme [9] used for coherent interfaces with significant misfit describes each inequivalent interface with a set of *identical* interface region supercells. This approach has been outlined schematically in Fig. 3a. It follows that, for a slab geometry of the type shown in Fig. 3c, and using (1):

$$\sigma = (1/A_P^{Slab})\{2N_{\mathbf{a}}A_0^{\mathbf{ab}}\sigma_0^{\mathbf{ab}} + 2N_{\mathbf{c}}A_0^{\mathbf{cb}}\sigma_0^{\mathbf{cb}}\}. \qquad (2)$$

The interface plane basis vectors of Fig. 3c have been used here for labeling the two contributions on the right hand side of (2). $N_{\mathbf{a}}$, $N_{\mathbf{c}}$ denote the number of interface region supercells needed to cover each inequivalent interface, '**ab**', '**cb**', respectively. Note that contributions from two interfaces are to be counted at a precipitate corner, i.e., for the precipitate in Fig. 3c, $N_{\mathbf{a}} = N_{\mathbf{c}} = 5$. The parameters $A_0^{\mathbf{ab}}$, $A_0^{\mathbf{cb}}$ refer to the areas of interface segments covered by a single cell. For consistency in the modeling, one must require $A_{\mathrm{P}}^{\mathrm{Slab}} = 2N_{\mathbf{a}}A_0^{\mathbf{ab}} + 2N_{\mathbf{c}}A_0^{\mathbf{cb}}$. The subscript in e.g. $\sigma_0^{\mathbf{ab}}$ emphasizes that the calculations employ interface region supercells with fully relaxed structural parameters ('zero' shear, see Sec. 2.4). The two interfacial energy contributions $\sigma_0^{\mathbf{ab}}$, $\sigma_0^{\mathbf{cb}}$ are dependent on both the chosen interface region size and the selected interface configuration. For simplicity, these dependencies are suppressed here.

By contrast, for the scheme proposed in this work, all supercells in the patchwork are different – distorted according to their location on the interface. Fig. 3b, 3c describe this approach schematically, with 10 different supercells needed for the modeling of the system in Fig. 3c. For a general slab of this type, the interfacial energy expression (2) should now be replaced by [12]:

$$\sigma = (1/A_P^{\mathrm{Slab}})\{\textstyle\sum_i 2A_i^{\mathbf{ab}}\sigma_i^{\mathbf{ab}} + \sum_j 2A_j^{\mathbf{cb}}\sigma_j^{\mathbf{cb}}\};$$
$$i = \{-N_{\mathbf{a}}/2; \ldots; N_{\mathbf{a}}/2\},\ j = \{-N_{\mathbf{c}}/2; \ldots; N_{\mathbf{c}}/2\}, \qquad (3)$$

with the interface area given as

$$A_{\mathrm{P}}^{\mathrm{Slab}} = \textstyle\sum_i 2A_i^{\mathbf{ab}} + \sum_j 2A_j^{\mathbf{cb}}; \qquad \text{(summing over } i, j \text{ as in (3))}. \qquad (4)$$

In these expressions, the labels i and j run over the horizontally (**ab**) and vertically (**cb**) oriented interfaces for the Fig. 3c type system, respectively. The individual interfacial energy contributions $\sigma_i^{\mathbf{ab}}$ are defined in the usual manner [9,10]:

$$\sigma_i^{\mathbf{ab}}(\mathbf{a}_i^{\mathbf{ab}}, \mathbf{b}_i^{\mathbf{ab}}, \mathbf{c}_i^{\mathbf{ab}}) = (1/(2A_i^{\mathbf{ab}}))\{E_{\mathrm{PH}}(\mathbf{a}_i^{\mathbf{ab}}, \mathbf{b}_i^{\mathbf{ab}}, \mathbf{c}_i^{\mathbf{ab}})$$
$$- (N_{\mathrm{P}}^{\mathbf{ab}}/N^{\mathbf{ab}})E_{\mathrm{P}}(\mathbf{a}_i^{\mathbf{ab}}, \mathbf{b}_i^{\mathbf{ab}}, \alpha_i^{\mathbf{ab}}\mathbf{c}_i^{\mathbf{ab}})$$
$$- (N_{\mathrm{H}}^{\mathbf{ab}}/N^{\mathbf{ab}})E_{\mathrm{H}}(\mathbf{a}_i^{\mathbf{ab}}, \mathbf{b}_i^{\mathbf{ab}}, \beta_i^{\mathbf{ab}}\mathbf{c}_i^{\mathbf{ab}})\}, \qquad (5)$$

with the expression for $\sigma_j^{\mathbf{cb}}$ being conceptually equivalent:

$$\sigma_j^{\mathbf{cb}}(\mathbf{a}_j^{\mathbf{cb}}, \mathbf{b}_j^{\mathbf{cb}}, \mathbf{c}_j^{\mathbf{cb}}) = (1/(2A_j^{\mathbf{cb}}))\{E_{\mathrm{PH}}(\mathbf{a}_j^{\mathbf{cb}}, \mathbf{b}_j^{\mathbf{cb}}, \mathbf{c}_j^{\mathbf{cb}}) - (N_{\mathrm{P}}^{\mathbf{cb}}/N^{\mathbf{cb}})E_{\mathrm{P}}(\alpha_j^{\mathbf{cb}}\mathbf{a}_j^{\mathbf{cb}}, \mathbf{b}_j^{\mathbf{cb}}, \mathbf{c}_j^{\mathbf{cb}}) - (N_{\mathrm{H}}^{\mathbf{cb}}/N^{\mathbf{cb}})E_{\mathrm{H}}(\beta_j^{\mathbf{cb}}\mathbf{a}_j^{\mathbf{cb}}, \mathbf{b}_j^{\mathbf{cb}}, \mathbf{c}_j^{\mathbf{cb}})\}. \quad (6)$$

For each equation from the pair (5), (6), E_{PH} denotes the total energy of the interface region supercell for the position on the interface characterized by the basis vector subscripts. The total energies E_{P}, E_{H} are those of bulk precipitate and host lattice systems, respectively, containing the same number of atoms as the interface region supercell, but with the cell dimensions constrained as described [13]. The parameters $\alpha_i^{\boldsymbol{x}\mathbf{b}}$, $\beta_i^{\boldsymbol{x}\mathbf{b}}$ (with $\boldsymbol{x}$ = **a** in (5) and $\boldsymbol{x}$ = **c** in (6)) are variables, i.e., only the direction is fixed for the basis vector out of the interface plane. The numbers $N_{\mathrm{P}}^{\boldsymbol{x}\mathbf{b}}$, $N_{\mathrm{H}}^{\boldsymbol{x}\mathbf{b}}$ refer to the number of precipitate and host lattice atoms, respectively, present in the interface region supercell ($N^{\boldsymbol{x}\mathbf{b}}$ atoms), i.e., $N^{\boldsymbol{x}\mathbf{b}} = N_{\mathrm{P}}^{\boldsymbol{x}\mathbf{b}} + N_{\mathrm{H}}^{\boldsymbol{x}\mathbf{b}}$.

In the case of the strain energy, as indicated in Sec. 1, the conventional scheme normally does not assume a spatially confined strain field. By contrast, our proposed scheme for simplicity (see Sec. 3.3 for details) calculates the strain energy only within the supercells underlying (3). The most acceptable comparison of the two schemes will evidently be attained when selecting the *same* strain field spatial confinement throughout. For this reason, we shall discuss first how the strain energy is derived in the new scheme, subsequently modifying these expressions to comply with the approximations of the conventional scheme.

For the model scheme proposed in this work, the strain energy is obtained by summing the weighted contributions from the individual supercells as:

$$\zeta = (1/N_{\mathbf{c}}N^{\mathbf{cb}} + N_{\mathbf{a}}N^{\mathbf{ab}})\{\textstyle\sum_i N^{\mathbf{ab}}\zeta_i^{\mathbf{ab}} + \sum_j N^{\mathbf{cb}}\zeta_j^{\mathbf{cb}}\}; \quad i = \{-N_{\mathbf{a}}/2; \ldots; N_{\mathbf{a}}/2\},\ j = \{-N_{\mathbf{c}}/2; \ldots; N_{\mathbf{c}}/2\}, \quad (7)$$

Here, following earlier definitions, the value of $N_{\mathbf{c}}N^{\mathbf{cb}} + N_{\mathbf{a}}N^{\mathbf{ab}}$ amounts to the number of atoms present within the added supercells. The strain energy contribution from individual supercells for the ab and cb interfaces is obtained [9,10] as

$$\zeta_i^{\mathbf{ab}}(\mathbf{a}_i^{\mathbf{ab}}, \mathbf{b}_i^{\mathbf{ab}}, \mathbf{c}_i^{\mathbf{ab}}) = (N_{\mathrm{P}}^{\mathbf{ab}}/N^{\mathbf{ab}})\{E_{\mathrm{P}}(\mathbf{a}_i^{\mathbf{ab}}, \mathbf{b}_i^{\mathbf{ab}}, \alpha_i^{\mathbf{ab}}\mathbf{c}_i^{\mathbf{ab}}) - E_{\mathrm{P}}\} + (N_{\mathrm{H}}^{\mathbf{ab}}/N^{\mathbf{ab}})\{E_{\mathrm{H}}(\mathbf{a}_i^{\mathbf{ab}}, \mathbf{b}_i^{\mathbf{ab}}, \beta_i^{\mathbf{ab}}\mathbf{c}_i^{\mathbf{ab}}) - E_{\mathrm{H}}\}, \quad (8)$$

$$\zeta_j^{\mathbf{cb}}(\mathbf{a}_j^{\mathbf{cb}}, \mathbf{b}_j^{\mathbf{cb}}, \mathbf{c}_j^{\mathbf{cb}}) = (N_{\mathrm{P}}^{\mathbf{cb}}/N^{\mathbf{cb}})\{E_{\mathrm{P}}(\alpha_j^{\mathbf{cb}}\mathbf{a}_j^{\mathbf{cb}}, \mathbf{b}_j^{\mathbf{cb}}, \mathbf{c}_j^{\mathbf{cb}}) - E_{\mathrm{P}}\} + (N_{\mathrm{H}}^{\mathbf{cb}}/N^{\mathbf{cb}})\{E_{\mathrm{H}}(\beta_j^{\mathbf{cb}}\mathbf{a}_j^{\mathbf{cb}}, \mathbf{b}_j^{\mathbf{cb}}, \mathbf{c}_j^{\mathbf{cb}}) - E_{\mathrm{H}}\}, \quad (9)$$

respectively. All parameters in these expressions have been explained in the paragraph following (6). The absence of any basis vector information for a given energy in (8), (9) indicates that a full relaxation of the system be performed.

Within the conventional scheme and using the same spatial strain field confinement, the contributions to ζ are also summarized according to (7), using the expressions (8), (9) for the individual $\zeta_i^{\mathbf{ab}}$, $\zeta_j^{\mathbf{cb}}$ terms, but with LET used throughout for the evaluation of the actual energy contributions. Along with (2), this stresses the usual limitations of the conventional scheme: the interfacial energy variation is always neglected and the strain field is never treated with *ab initio* theory (but only with LET).

Summarizing, it follows from (1) that the interface energy $E_{\mathrm{Int,\,new}} = \Delta H_{\mathrm{P}}^{SS} - \Delta H_{\mathrm{P,\,Bulk}}^{SS}$, as calculated within our proposed scheme and with the strain field spatial confinement underlying (7), is given as

$$E_{\mathrm{Int,\,new}} = \sum_i E^{\mathbf{ab}}{}_{\mathrm{Int,\,new},\,i} + \sum_j E^{\mathbf{cb}}{}_{\mathrm{Int,\,new},\,j} = \sum_i \{2A_i^{\mathbf{ab}}\sigma_i^{\mathbf{ab}} + N^{\mathbf{ab}}\zeta_i^{\mathbf{ab}}\} + \sum_j \{2A_j^{\mathbf{cb}}\sigma_j^{\mathbf{cb}} + N^{\mathbf{cb}}\zeta_j^{\mathbf{cb}}\}; \quad i = \{-N_{\mathbf{a}}/2; \ldots; N_{\mathbf{a}}/2\},\ j = \{-N_{\mathbf{c}}/2; \ldots; N_{\mathbf{c}}/2\}. \quad (10)$$

where e.g. $E^{\mathbf{ab}}{}_{\mathrm{Int,\,new},\,i}$ is the interface energy contribution from supercell i for the ab interface. By comparison, the corresponding quantity $E_{\mathrm{Int,\,conv.}}$ as derived within the conventional scheme with the same strain field confinement is given as

$$E_{\mathrm{Int,\,conv.}} = \sum_i E^{\mathbf{ab}}{}_{\mathrm{Int,\,conv.},\,i} + \sum_j E^{\mathbf{cb}}{}_{\mathrm{Int,\,conv.},\,j} = \sum_i \{2A_0^{\mathbf{ab}}\sigma_0^{\mathbf{ab}} + N^{\mathbf{ab}}\zeta_i^{\mathbf{ab}}\} + \sum_j \{2A_0^{\mathbf{cb}}\sigma_0^{\mathbf{cb}} + N^{\mathbf{cb}}\zeta_j^{\mathbf{cb}}\};$$

$$i = \{-N_{\mathbf{a}}/2; \ldots; N_{\mathbf{a}}/2\},\ j = \{-N_{\mathbf{c}}/2; \ldots; N_{\mathbf{c}}/2\}, \qquad (11)$$

where the strain energy contributions are computed within LET.

3.3. Interface region supercell distortions

The key equations (3) and (7) in Sec. 3.2 for determination of the interfacial and strain energies of a system of the type shown in Fig. 3c are at this stage entirely formal expressions: the cell distortions defining the cells with $i, j \neq 0$ are yet to be discussed. As stressed in Sec. 2.4, the basic idea behind our model scheme is to make each cell distortion match the local strain of the interface region that this cell is intended to describe. Evidently, such a relation is closely connected to the subsystem misfits, hence requiring a structural coupling between the set of supercells and the remaining parts of the system, farther away from the interface. The most precise version of such a coupling in general involves an actual communication between these regions, followed by mutual adaption for self-consistency, i.e., a hybrid atomistic model scheme [14]. In this work, we choose the much simpler scenario of ignoring the influence of the interface region on the surrounding system. This leaves modeling outside of the supercell covered region unnecessary, as all remaining parts of the two subsystems are in their bulk state ($\zeta = 0$). The only task left is to establish the appropriate cell distortions compatible with this selected choice of state of the 'outside region'.

We use here a fundamental property of the fully coherent precipitate in a host lattice: in the absence of defects at the interface, it is possible to choose a bulk host lattice supercell with the basis vector directions essentially identical to those of the bulk precipitate. The argumentation may go as follows: in the hypothetical case of zero misfit between the subsystems along all directions, the two sets of basis vectors would evidently be identical. The presence of misfits limits this identity to an approximate one, for the *normalized* bulk basis vectors – and only if the accumulated strain along the interfaces does not promote defect formation, driving the system away from near perfection. The idealized identity, used below, hence reads:

$$\mathbf{a}_P/|\mathbf{a}_P| = \mathbf{a}_H/|\mathbf{a}_H|\ ;\ \mathbf{b}_P/|\mathbf{b}_P| = \mathbf{b}_H/|\mathbf{b}_H|\ ;\ \mathbf{c}_P/|\mathbf{c}_P| = \mathbf{c}_H/|\mathbf{c}_H|. \qquad (12)$$

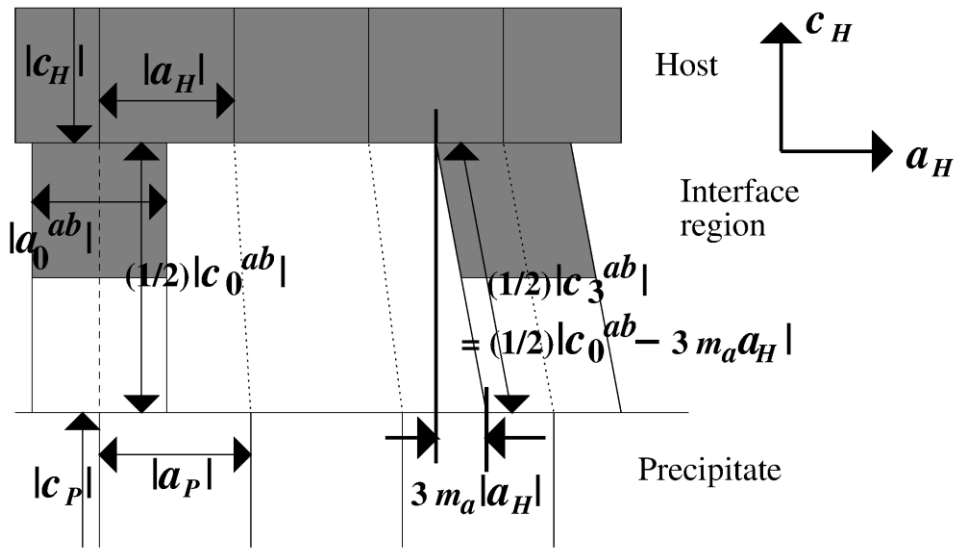

Fig. 4. Schematic presentation of the determination of the appropriate interface region supercell distortion. Two different supercells (halves, only one interface shown) are displayed: the cell describing the point of minimal strain on the interface (left), cell label $i = 0$, and a cell describing a distorted region along the interface (right), $i = -3$. See text for details.

Fig. 4 summarizes the picture emerging, showing (for the **ab** interface) how the supercell distortions can now be derived. Firstly, upon neglecting the strain field outside the region covered by supercells, the boundaries to this region will be planes (straight horizontal lines in Fig. 4). This follows from (12) and the general assumption that the interface will run parallel to the basis vectors shown [15]. Consequently, if one neglects – momentarily – variations with cell label i in the lengths of the interface region basis vectors in the interface plane $\mathbf{a}_i^{\mathbf{ab}}$, $\mathbf{b}_i^{\mathbf{ab}}$, the cell distortion when moving away from the point of minimal strain on this interface will be *pure shear strain*.

The boundary condition to the surrounding parts of the system also dictates the *magnitude* of this shear component as a function of the movement along the interface. We choose here a positive value of i to imply a change of $\mathbf{c}_i^{\mathbf{ab}}$ *toward* $\mathbf{a}_\mathrm{H}$. A movement by i interface region supercells in Fig. 4 amounts to a movement by the distance $i\mathbf{a}_\mathrm{H}$ in the bulk host lattice, but a movement by $i\mathbf{a}_\mathrm{P}$ in the bulk precipitate. The actual supercell has to satisfy both criteria (at the respective boundaries to host lattice and precipitate), and hence

$$\mathbf{c}_i^{\mathbf{ab}} = \mathbf{c}_0^{\mathbf{ab}} + 2im_\mathbf{a}\mathbf{a}_\mathrm{H}, \qquad (13)$$

where the multiplication by 2 comes from the fact that only half the cell is included in Fig. 4. Likewise, for the **cb** interface in Fig. 3c:

$$\mathbf{a}_i^{\mathbf{cb}} = \mathbf{a}_0^{\mathbf{cb}} + 2jm_{\mathbf{c}}\mathbf{c}_{\mathrm{H}}. \qquad (14)$$

Note that only the directions – not the lengths - can be assumed fixed in general for the interface region basis vectors lying in the two interface planes. Also, the arguments underlying the above picture are only consistent if the normalized basis vectors for the structurally optimized interface region supercells essentially satisfy (12). This is stressed for the case of $\mathbf{a}_0^{\mathbf{ab}}$, $\mathbf{c}_0^{\mathbf{ab}}$ in Fig. 4.

4. Selected test system: the β'' precipitate

4.1. Precipitate bulk and interface structure

The precipitate-host lattice system under investigation in the present paper is β"/Al. The β" phase is a fully coherent needle shaped precipitate, i.e., a physical example of the system displayed schematically in Fig. 3c. This precipitate is the main hardening phase in the industrially important Al–Mg–Si alloy system [16,17]. The structure of β" was identified more than a decade ago by Zandbergen *et al.* [6], but the composition is still debated, with recent experimental work by Hasting *et al.* [11] modifying the originally suggested Mg_5Si_6 composition [18] to $Mg_5Al_2Si_4$. In the present work, we shall address both compositions, discussing explicitly the structural requirements for a fully coherent phase presented in Sec. 3.3.

The β"/Al orientation relationships for the conventional monoclinic β" unit cell (22 atoms) are [18]:

$$[230]_{\mathrm{Al}} \parallel [100]_{\beta''}^{\mathrm{Conv.}};\ [001]_{\mathrm{Al}} \parallel [010]_{\beta''}^{\mathrm{Conv.}};\ [\bar{3}10]_{\mathrm{Al}} \parallel [001]_{\beta''}^{\mathrm{Conv.}}. \qquad (15)$$

For the primitive β" unit cell (11 atoms), which is related to the above conventional counterpart through $\mathbf{a}_{\beta''}^{\mathrm{Prim.}} = (½)\{\mathbf{a}_{\beta''}^{\mathrm{Conv.}} + \mathbf{b}_{\beta''}^{\mathrm{Conv.}}\}$ [18], the first orientation relation in (15) is changed into:

$$[231]_{\mathrm{Al}} \parallel [100]_{\beta''}^{\mathrm{Prim.}}. \qquad (16)$$

Given the $\mathbf{b}_{\beta''}$ and $\mathbf{c}_{\beta''}$ basis vector identities for the conventional and primitive cells, the basis vector

superscript is used only for $\mathbf{a}_{\beta''}$ below. For computational simplicity, our calculations employ interface region supercells connected with the β" primitive cell throughout. However, when comparing with experimental information, we use the corresponding conventional cells. The main growth (needle axis) direction of β" is along $\mathbf{b}_{\beta''}$, with the experimentally reported [18] β"/Al misfit values along $\mathbf{a}_{\beta''}^{Conv.}$, $\mathbf{b}_{\beta''}$ and $\mathbf{c}_{\beta''}$ being 3.8%, 'vanishing' and 5.3%, respectively. A schematic presentation of the β" primitive cell has been included in Fig. 5a.

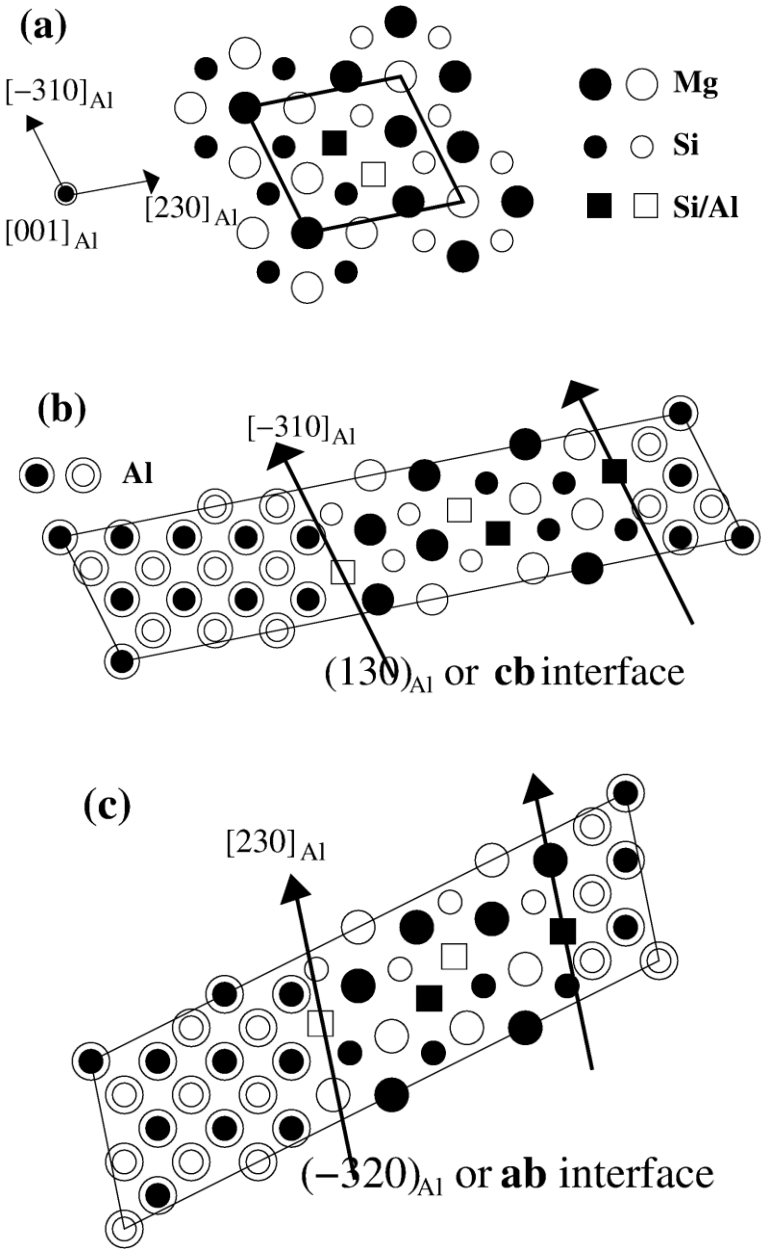

Fig. 5. Schematic illustration of selected β" and β"/Al cells investigated in the present work: (a) Bulk β" primitive unit cell. The two configurations considered – compositions $Mg_5Al_2Si_4$, Mg_5Si_6 – have both been included by highlighting the atoms of 'varying type'. The precipitate main growth

axis direction $[001]_{Al}$ ($\mathbf{b}_{\beta''}$) is out of the paper. Black and white atoms are located at different heights (separation 2.025 Å). For the β"/Al orientation relationships, see (15), (16). (b) Selected interface configuration for the $(130)_{Al}$ interface (stoichiometric precipitate with equivalent interfaces). Structural relaxations have been neglected in the figure for both subsystems. (c) Selected interface configuration for the $(–320)_{Al}$ interface (same overall criteria as in (b)).

Both the interface region supercells under investigation (see Fig. 5b, 5c) are 44 atom unit cells, corresponding to four primitive β" unit cells (compare with Fig. 5a), extended along either $\mathbf{a}_{\beta''}^{Prim.}$ ($(130)_{Al}$ interface) or $\mathbf{c}_{\beta''}$ ($(–320)_{Al}$ interface). In the notation of Sec. 3, these are the **cb** and **ab** interfaces, respectively. Our cell size choice follows the work by Wang *et al.* in [9] in the context of interface region width: the authors of [9] concluded that interfacial energies were essentially converged for 44 atom supercells in the case of a stoichiometric precipitate with composition Mg_5Si_6 and identical interface configurations for the two interfaces of same orientation. We choose identical interface configurations compatible with a stoichiometric precipitate as well, as the expressions (5), (6), (8) and (9) defining the local interfacial and strain energies are ill-defined otherwise. The stoichiometry implies that e.g., $N_P^{\mathbf{ab}} = N_H^{\mathbf{ab}} = (1/2)N^{\mathbf{ab}}$.

4.2. Subsystem elastic constants

Following e.g. Kittel [19], the deformation energy ΔE of a bulk unit cell can generally be described within LET as:

$$\Delta E = E_0 + (V_0/2)\sum_i\sum_j c_{ij}e_ie_j; \qquad i, j = \{1; ...; 6\}. \qquad (17)$$

Here, E_0 and V_0 represent the total energy and cell volume, respectively, for the fully relaxed system. The parameters c_{ij} are the system elastic constants, and the quantities e_i describe the level of structural deformation, as calculated in a basis of initially orthonormal vectors $\{\mathbf{x}, \mathbf{y}, \mathbf{z}\} \rightarrow \{\mathbf{x}', \mathbf{y}', \mathbf{z}'\}$, with e.g. e_1 ($= e_{xx}$) $= \mathbf{x}' \cdot \mathbf{x}' - \mathbf{x} \cdot \mathbf{x}$. Accounting for all permutations among the basis vectors, summations in (17) will span the values $i = 1, ... , 6$ (same for j) [20]. For face-centered cubic (fcc) Al, structural symmetries reduce the number of independent elastic constants to 3; c_{11}, c_{12} and c_{44}. For monoclinic β", there are 13 such constants to determine (as discussed in Sec. 5.3, a smaller number suffices for the considerations of the present work). The calculated elastic constants are presented in Sec. 5.3.

4.3. Computational details

The calculations of the present work have been performed within the framework of density functional theory (DFT) [21,22]. In practice, we employed Vanderbilt ultrasoft pseudopotentials [23] as implemented in the plane wave (PW) based Vienna *Ab initio* Simulation Package (VASP) [24,25]. The Perdew-Wang generalized gradient approximation (GGA) to the exchange-correlation functional [26] was applied throughout. As the majority of our studies considered distortions of systems away from their fully relaxed state, and as such studies have been shown to have a tendency for higher precision requirements, compared to full optimization considerations (see e.g. [27]), we have taken care to both select a high precision and ensure that our results were acceptably converged. For all studies included in the paper, a comparatively high PW energy cut-off value of 225 eV (for a system containing Mg, Si and Al) was used, along with a (12, 22, 14) *k*-point grid for the primitive β" and related Al supercell studies, and compatible (12/*n*, 22, 14/*m*) *k*-point grids whenever possible for the interface regions extended along either $\mathbf{a}_{\beta"}^{\text{Prim.}}$ (*n*) or $\mathbf{c}_{\beta"}$ (*m*). Additional studies involving more dense (16/*n*, 32, 18/*m*) *k*-point grids indicated practically converged structural parameters and energies. The Al elastic constants were determined using a conventional fcc unit cell and a (22, 22, 22) *k*-point grid.

For the β"/Al supercell distortions, we chose to let only $c_i^{\mathbf{ab}}$, $a_j^{\mathbf{cb}}$ display variations – as dictated by (13), (14) – with movements away from the center of each respective interface. In other words (see Sec. 3.3), the cell distortions were always pure shear strain. For the two most strongly distorted cells on each interface, remaining basis vector lengths were optimized in additional studies to address the level of errors connected with the above simplification. We found the distortion energies in these studies to be altered by no more than a few percent, hence accepting the chosen scheme as sufficiently reliable for further analysis. The full set of β"/Al basis vectors and calculated interface energies have been described in Table A1, A2 of App. A.

For the determination of the interfacial and strain energies, we assumed for simplicity $\alpha_i^{\mathbf{ab}} = \alpha_0^{\mathbf{ab}}$, $\beta_i^{\mathbf{ab}} = \beta_0^{\mathbf{ab}}$ in (5), (8) (and, correspondingly, $\alpha_j^{\mathbf{cb}} = \alpha_0^{\mathbf{cb}}$, $\beta_j^{\mathbf{cb}} = \beta_0^{\mathbf{cb}}$ in (6), (9)), as opposed to optimizing these parameters for each new distorted cell. The values of these parameters have been provided in App. A. As the resulting cell energy changes for e.g. the ab interface consideration are subtracted in (5) but added in (8), any errors related to the present simplification would lead to an

incorrect division of the total interface energy into the strain and interfacial energy components. These errors were evaluated in the same manner as described in the previous paragraph: we found that the strain (interfacial) energy was at most modified by ≈ 0.03 kJ/mol at. (≈ 2 mJ/m²), once again a few percent of the total variation. Consequently, also this simplification was concluded acceptable. The strain energies thus determined have been included in App. A (Table A3, A4).

5. Results and discussion

5.1. Bulk phases

The calculated cell dimensions and total energies for bulk Al and β"–Mg_5Si_6, β"–$Mg_5Al_2Si_4$ have been included in Table 1. Compared to experiment, the Al lattice parameter is a few tenths of a percent *below* the reported value of 4.05Å at ambient conditions while most values for the β" cell dimensions (both compositions) are *above* their experimental counterparts. The theoretical bulk subsystem misfit values obtained consequently tend to exceed the experimental values included in Sec. 4.1. We find

$m_{\mathbf{a}} = 3.7\%$; $m_{\mathbf{b}} = 0.9\%$; $m_{\mathbf{c}} = 8.4\%$ (β"–Mg_5Si_6); (18)

$m_{\mathbf{a}} = 5.0\%$; $m_{\mathbf{b}} = 0.8\%$; $m_{\mathbf{c}} = 6.0\%$ (β"–$Mg_5Al_2Si_4$). (19)

In (18), (19) we have regarded the slight scatter in the Al lattice parameter as a purely precision related error, using $a_{Al} = 4.044$ Å. It is conceivable that at least some of the discrepancy between theory and experiment should be attributed to the fact that calculations here refer to isolated, rather than interacting subsystems. In particular, the interactions would have a tendency to compress β".

Our main requirement for acceptable structural parameters in the context of the interface model scheme of Sec. 3.3 is not the calculated misfit values (18), (19), but the degree to which (12) is obeyed. In the context of the bulk precipitate, β"–$Mg_5Al_2Si_4$ performs markedly better than β"–Mg_5Si_6, given that the latter bulk phase has an angle of roughly 110° between basis vectors $\mathbf{a}_{\beta''}^{Conv.}$ and $\mathbf{c}_{\beta''}$, compared to the experimental value of 105-106° [18], while the former is essentially spot on (see Table 1). While this does not necessarily exclude Mg_5Si_6 as a candidate for the precipitate composition, we have made the choice to focus only on β"–$Mg_5Al_2Si_4$ in the remaining work.

Table 1. Cell dimensions of fully relaxed bulk Al and β" (two compositions) cells. Deviations from the relation $\mathbf{a}_{\beta''}^{\text{Prim.}} = (1/2)\{\mathbf{a}_{\beta''}^{\text{Conv.}} + \mathbf{b}_{\beta''}\}$ – used here for converting the output parameter from calculations $|\mathbf{a}_{\beta''}^{\text{Prim.}}|$ to the parameter $|\mathbf{a}_{\beta''}^{\text{Conv.}}|$ – are negligible throughout. For perfect fcc Al with lattice parameter 4.044 Å, the cell dimension values corresponding the first row differ by 0.005 Å or less.

System	$\lvert\mathbf{a}_{\beta''}^{\text{Conv.}}\rvert$ (Å)	$\lvert\mathbf{b}_{\beta''}\rvert$ (Å)	$\lvert\mathbf{c}_{\beta''}\rvert$ (Å)	β (°)
Al (β" supercell)	14.58	4.041	6.399	105.3
β"–Mg_5Si_6	15.11	4.080	6.932	110.4
β"–$Mg_5Al_2Si_4$	15.32	4.075	6.778	105.9

5.2. Interface configurations

In Table 2, the calculated cell dimensions for the two β"–$Mg_5Al_2Si_4$/Al interface region supercells describing the center of the $(130)_{Al}$ and $(–320)_{Al}$ interfaces (see Fig. 5b, 5c) have been included. For both interfaces, the fully relaxed basis vector angles closely match those of bulk β"–$Mg_5Al_2Si_4$ and the Al supercell of Table 1. In other words, (12) is essentially satisfied also for the interface regions, and from this perspective, the choice of interface configurations appears acceptable.

Table 2. Cell dimensions of fully relaxed 44 atom β"–$Mg_5Al_2Si_4$/Al supercells describing interfaces with normal vectors $\mathbf{n}^{\mathbf{cb}} = (130)_{Al}$ and $\mathbf{n}^{\mathbf{ab}} = (–320)_{Al}$. The remarks from Table 1 on basis vector conversion apply here as well. By construction of the supercells (see Fig. 5b, 5c), the basis vectors $\mathbf{a}_0^{\mathbf{cb}}$, $\mathbf{c}_0^{\mathbf{ab}}$ pointing out of interface planes have lengths roughly matching the sum of two bulk Al supercell and two β" primitive cell basis vectors of the same type (see Table 1).

Interface orient. (ij)	$\lvert\mathbf{a}_0^{ij}\rvert$ (Å)	$\lvert\mathbf{b}_0^{ij}\rvert$ (Å)	$\lvert\mathbf{c}_0^{ij}\rvert$ (Å)	β_0^{ij} (°)
$(130)_{Al}$ (**cb**)	59.83	4.048	6.619	105.5
$(–320)_{Al}$ (**ab**)	15.05	4.006	26.61	105.4

We note that the predicted misfit value along the precipitate main growth direction for the $(–320)_{Al}$ interface region does not appear to agree well with the experimentally reported negligible misfit (which would suggest $\mathbf{b}_0^{\mathbf{ab}} \approx 4.05$ Å). This issue is possibly connected with the non-negligible

misfit between the two bulk subsystems along the same direction (see Table 1) – though it is also noted that the misfit is found to be absent for the $(130)_{Al}$ interface region. In summary, we can not conclude from the results in Table 2 that the interface configuration choice is problematic, as it might be the chosen bulk precipitate composition that should be modified.

Table 3. Calculated elastic constants for bulk fcc Al and monoclinic β"–$Mg_5Al_2Si_4$. The values of E_0, V_0 for Al and β", used in (17) for deducing these constants, are {–5.916 (10^{19} J/atom); 16.53 (10^{30} m³/atom)} and {–5.4542; 18.54}, respectively.

Elastic constant	Al (10^{11} N/m²)	β"–$Mg_5Al_2Si_4$ (10^{11} N/m²)
c_{11}	1.0387	1.0897
c_{22}	(= c_{11})	0.8963
c_{33}	(= c_{11})	0.9875
c_{12}	0.6001	0.4936
c_{13}	(= c_{12})	0.4308
c_{23}	(= c_{12})	0.5770
c_{44}	0.2936	(-)
c_{55}	(= c_{44})	0.2751

5.3. Subsystem elastic constants

The calculated elastic constants for bulk fcc Al and monoclinic β"–$Mg_5Al_2Si_4$, needed for the investigations of the present work, are displayed in Table 3. Given the interface region supercell optimization results (Sec. 5.2) and the choice of supercell distortions (Sec. 4.3), only 7 out of the full 13 elastic constants for β" were needed here – c_{11}, c_{22}, c_{33}, c_{12}, c_{13}, c_{23} and c_{55}. The first 6 constants are connected with the modification of the lengths, but with preservation of directions for the interface region basis vectors, encountered (almost perfectly) upon full optimization. The last constant c_{55} is needed to evaluate the effects of the added supercell shear strain when moving away from the interface center. For the Al subsystem, all three elastic constants c_{11}, c_{12} and c_{44} were needed. With exception of c_{11}, the precipitate is softer than Al according to the calculations, and markedly so (> 10%, c_{22}) along $b_{\beta''}$.

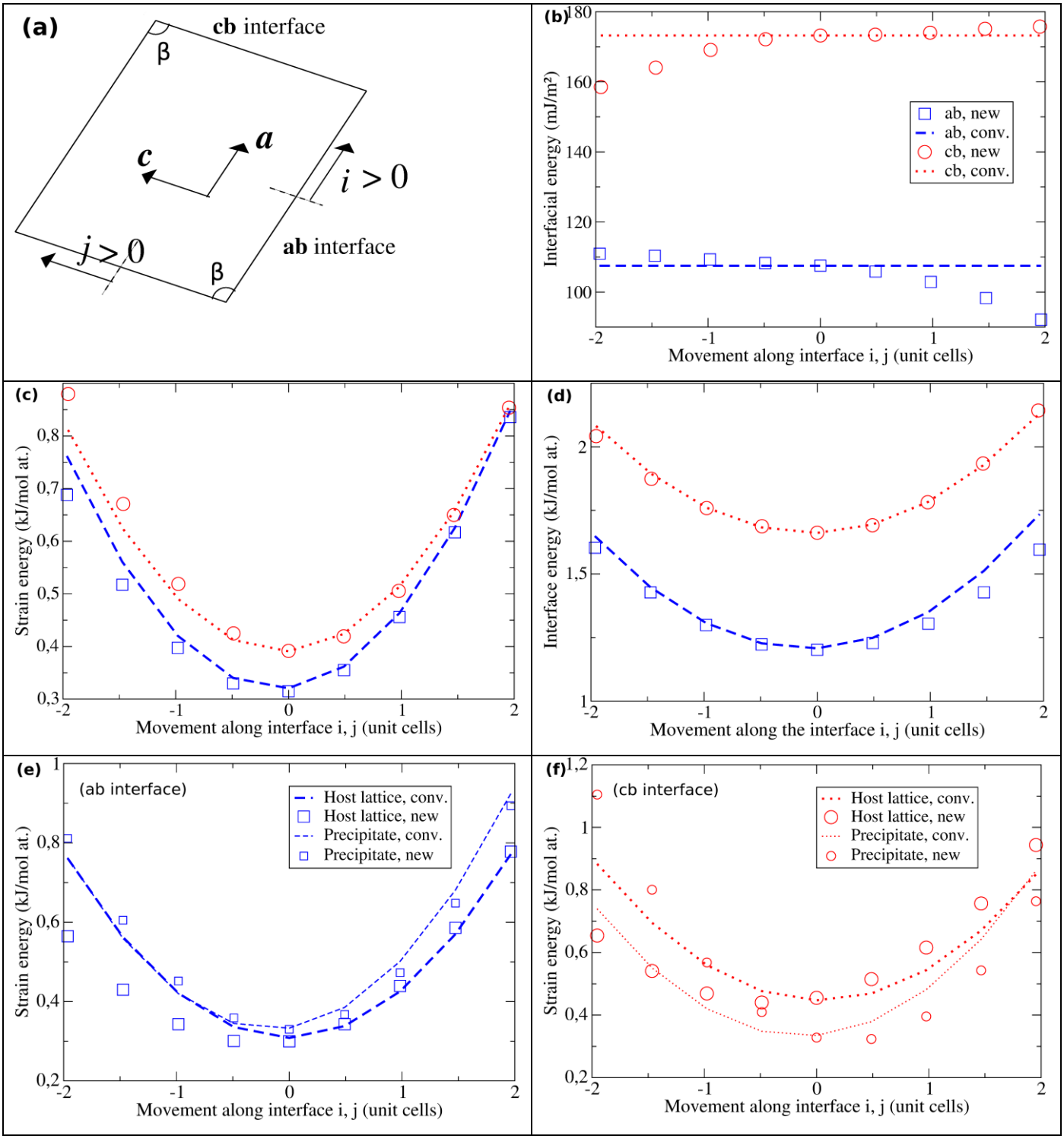

Fig. 6. Calculated variations of interfacial and strain energies for the β"–$Mg_5Al_2Si_4$/Al system. (a) Schematic illustration of the connection between the parameters *i*, *j* used in (b) – (e) and the position on the β"/Al interface. (b) The interfacial energy contributions $\sigma_i^{\mathbf{ab}}$, $\sigma_j^{\mathbf{cb}}$, as a function of movements along the β"–$Mg_5Al_2Si_4$/Al $(-320)_{Al}$ (**ab**) and $(130)_{Al}$ (**cb**) interfaces, respectively, obtained using (5), (6). In the conventional scheme, $\sigma_i^{\mathbf{ab}} = \sigma_0^{\mathbf{ab}}$; $\sigma_j^{\mathbf{cb}} = \sigma_0^{\mathbf{cb}}$. (c) The strain energy contributions $\zeta_i^{\mathbf{ab}}$, $\zeta_j^{\mathbf{cb}}$, obtained using (8), (9). For the conventional scheme, LET was used. (d)

Interface energy contributions $E^{\mathbf{ab}}_{\text{Int, new, }i}$, $E^{\mathbf{cb}}_{\text{Int, new, }j}$ (10) and $E^{\mathbf{ab}}_{\text{Int, conv., }i}$, $E^{\mathbf{cb}}_{\text{Int, conv., }j}$ (11), as obtained within the new and conventional scheme respectively. (e) Individual subsystem (Al, β") contributions to the strain energy along the **ab** interface. (f) Same, along the **cb** interface.

5.4. Interfacial and strain energies

A schematic illustration of the β" precipitate is shown in Fig. 6a, where the directions of *i* and *j* used for the supercell labeling are related to the unit cell monoclinic angle β. Following the definition of the direction of increasing *i* in Sec. 3.3, we find that the lowest *i* values are located at the β corner, with the same conclusion applying to *j*. The calculated interfacial energies for the β"–$Mg_5Al_2Si_4$/Al $(130)_{Al}$ and $(–320)_{Al}$ interfaces as a function of position on the β" needle cross section region are displayed in Fig. 6b, with the corresponding strain energies included in Fig. 6c. Results obtained with both the new and conventional schemes have been shown. Within the conventional scheme, $\sigma_i^{\mathbf{ab}}$, $\sigma_j^{\mathbf{cb}}$ are both assumed constant, equal to the value at the respective interface centers, whereas a weak, numerically similar variation spanning a range of ≈ 20 mJ/m² is noted for both of these quantities when using the scheme of the present work. The value of $\sigma_i^{\mathbf{ab}}$ is found to monotonically decrease for $i > 0$, while remaining almost constant for $i < 0$. For the case of $\sigma_j^{\mathbf{cb}}$, the decrease is in the direction of negative *j*. Comparing with Fig. 6a, this implies that the energetically most favorable configurations from the two different interfaces are located at different corners of the precipitate. These variations are relatively small, amounting to ≈ 10% (20%) of the value of $\sigma_0^{\mathbf{ab}}$ ($\sigma_0^{\mathbf{cb}}$). In other words, the conventional and new schemes compare rather well for the interfacial energy.

Differences between the results of the two schemes are likewise fairly weak when turning to the strain energies: here, the agreement of the DFT based and LET results is essentially perfect for $i, j > 0$, with differences increasing to ≈ 10% (0.06 – 0.07 kJ/mol at.) at the most negative values of *i, j*. Notably, the DFT strain energies are below the LET ones for the case of the $(–320)_{Al}$ interface, $\zeta_i^{\mathbf{ab}}$, but above them for the case of the $(130)_{Al}$ interface, $\zeta_j^{\mathbf{cb}}$. The variation in the full interface energy, shown in Fig. 6d, is found to be more symmetric around the interface center than any of the interfacial and strain energy variations. In other words, the DFT asymmetries around $i, j = 0$ in Fig. 6b, c largely cancel out here.

5.5. Analysis of the results

Experiment [28] reports typical β" cross section dimensions of ≈ 4 × 4 nm – corresponding to a cross section size in terms of unit cells $N_{\mathbf{a}} \times N_{\mathbf{c}} \approx 5 \times 6$. As this range is almost fully covered by Fig. 6b, c, it appears evident that the conventional scheme of Sec. 3.2 is capable of predicting acceptably the values of σ and ζ, within the model approximations of the present work (the actual variation in these quantities with precipitate size is discussed below). The question remaining to be discussed concerns the influence of these chosen approximations on the similarity of the two scheme predictions.

The unphysical confinement of the strain field to the interface region is an action performed in the conventional scheme only for the sake of optimal comparability with the new model scheme introduced in Sec. 3.2: in other words, both schemes adopt, for simplicity, the same structural boundary condition to the remaining parts of the β"/Al system. Given the close agreement between the strain energies within the interface region under these constraints (Fig. 6c), relaxing the strain field confinement might be expected to introduce only weak differences between the two sets of strain energies. However, a separation of the strain energy into individual subsystem contributions (Fig. 6e, f) yields a different conclusion. In Fig. 6e, we have divided the parameter $\zeta_i^{\mathbf{ab}}$ into the two contributions in (8), omitting the front factors (weights) $N_{\mathrm{P}}^{\mathbf{ab}}/N^{\mathbf{ab}}$, $N_{\mathrm{H}}^{\mathbf{ab}}/N^{\mathbf{ab}}$ for these terms. The same procedure was followed in Fig. 6f for $\zeta_j^{\mathbf{cb}}$ of (9). It is evident from this consideration that the close agreement between the two model scheme results in Fig. 6c hides considerably larger differences at the individual Al and β" level.

In order to clarify the importance of these discrepancies between the scheme predictions, we plotted (Fig. 7a) the strain energy variation with precipitate cross section size, using (7), and further divided this quantity into subsystem contributions by substituting the strain energy contributions $\zeta_i^{\mathbf{ab}}$, $\zeta_j^{\mathbf{cb}}$ with the subsystem contribution of interest, in the same manner as described above (Fig. 7b, c). As expected from Fig. 6c, the results obtained with the two schemes in Fig. 7a are practically negligible. By contrast, at typical experimental [28] β" cross section sizes, the (weakly extrapolated) DFT Al strain energy contribution in Fig. 7b is now ≈ 6% below the linear elasticity result, while the DFT β" strain energy contribution is ≈ 5% above the LET prediction.

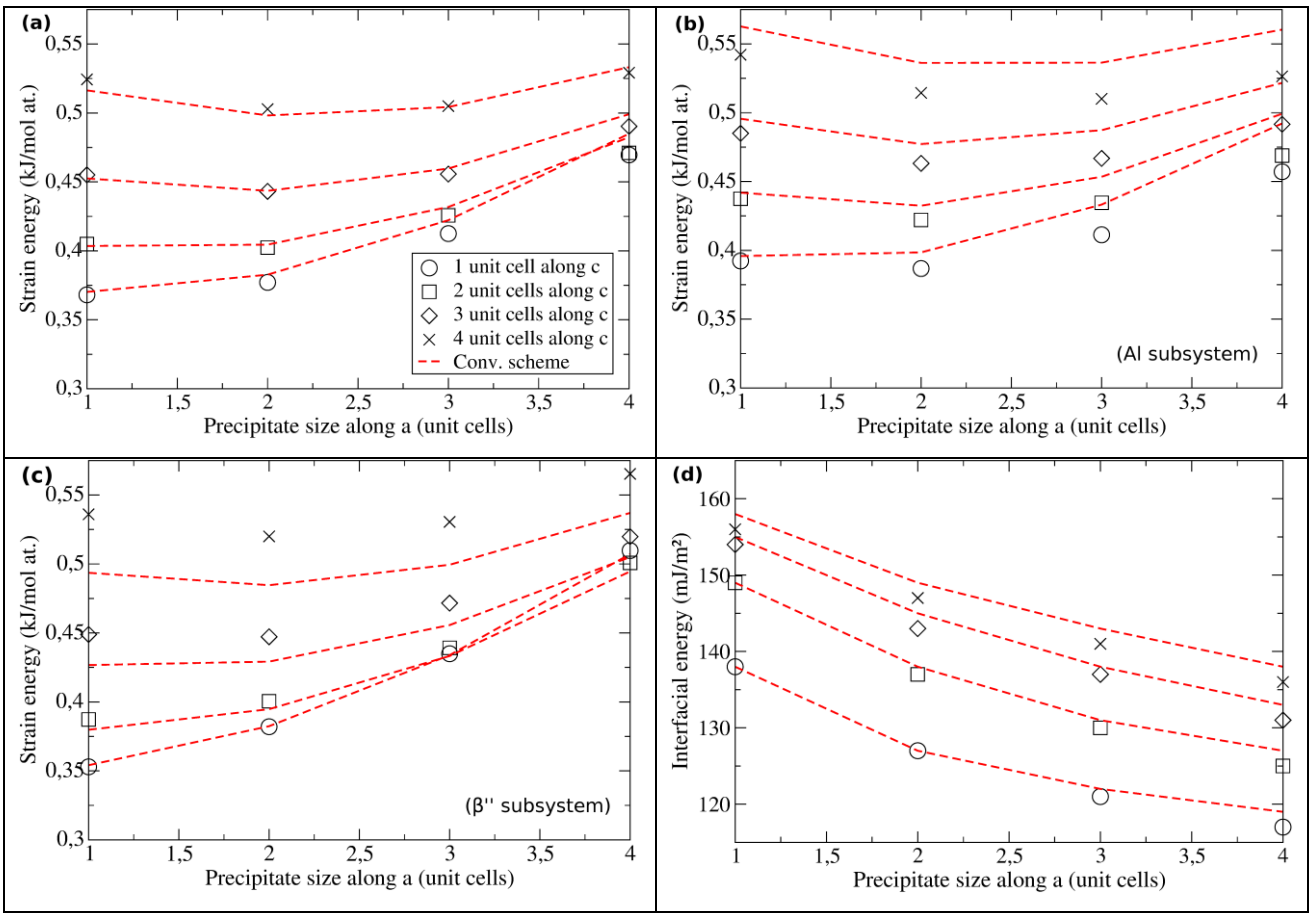

Fig. 7. (a) Calculated variation of the full strain energy ζ as a function of precipitate cross section size, obtained using (7). (b), (c) Subsystem (Al, β") contributions to the result in (a), see text for details. (d) Calculated variation in the full interfacial energy σ as a function of precipitate cross section size, obtained using (2), (3) for the conventional and new scheme, respectively.

We consider this observation of a non-negligible cancellation of errors in Fig. 7a important for the following reason: the supercells describing the two interface region centers – the cells upon which all the remaining interface region cells are constructed, see (13), (14) – are presently optimized without any constraints relating to the full β"/Al system (see Sec. 2.4). This choice of starting point is made for the sake of convenience, rather than accuracy. If the ultimate target of the model scheme – a self-consistent structural boundary condition to the remaining parts of the β"/Al system – were implemented, these supercell dimensions would almost certainly be significantly affected: contrasting the full optimization procedure of Sec. 2.4, in particular, the precipitate would now likely be subjected to compressive strain along *both* cross section basis vector directions. The results of Fig. 6e, f strongly support our suspicion (Sec. 1) that LET is unable to deal truly satisfactorily with the strain evolution along the coherent and highly misfit **ab** and **cb** interfaces. This in turn implies that the comparability of the strain energy predictions for the conventional and

new schemes is closely connected with the influence of improvements of the latter scheme: one should be cautious about concluding that the two schemes will always compare well.

The calculated variation in the interfacial energy σ with precipitate cross section size, as obtained with the conventional and new schemes, using (2) and (3), respectively, is shown in Fig. 7d. Despite the weak differences between the two sets of results, the question of the interfacial energy sensitivity to structural boundary condition modifications is in a sense even more pressing than the strain energy discussion. In the conventional scheme, the determination of σ makes general reference to the constraint-free optimization of the interface region supercell, hence being unaffected by the exact treatment of the strain energy. If σ were strongly altered in our new scheme upon implementation of a more physical boundary condition, this change would remain entirely neglected in (2). Of course, this statement should be balanced with the relatively weak variations in $\sigma_i^{\mathbf{ab}}$, $\sigma_j^{\mathbf{cb}}$ encountered in the present work (Fig. 6b). The issue of σ sensitivity to cell distortions should be fully addressed as well, but may not be a crucial matter.

5.6. Applications and limitations of the model scheme

The model scheme presented in this work offers a robust and computationally highly feasible way to determine the interface energy of a physically sized fully coherent precipitate in a host lattice within an *ab initio* based theoretical framework. For simplicity, the paper has focused on outlining the basic ideas underlying the method in their simplest approximated form. At the same time, we have indicated the potential simplicity of the improvement of the scheme to a more realistic scenario where the long range parts of the strain field are included in the model description. Implementation of our methodology in a hybrid atomistic scheme would seemingly involve only a modification of the structural boundary conditions (13), (14) to a more physically acceptable (self-consistent) condition. Further, as is usual for such hybrid schemes [14], it would be the expectation that calculations outside the interface region would be clearly less computationally intensive. Future work will address this topic in more detail.

More generally speaking, the model scheme provides the ability to probe most local regions on the precipitate-host lattice interface directly, opening the door to a series of potentially interesting topics of investigation. Interface configuration stabilities can now be addressed in closer detail, with the obvious potential effects on the calculated interfacial and strain energies. Ultimately, this means that

also precipitate stabilities (in the context of new phases nucleating on existing ones) can in principle be investigated.

A key outstanding issue at present involves the ability of our proposed model scheme to perform decisively better than presently available [5,9] – and less computationally demanding – schemes where the strain evolution along the interface is computed using LET. We make a note of this topic in the present section, as the analysis of Sec. 5.5 has failed to provide a full answer to the question of the general comparability of the two schemes. Arguably, in the context of a precise determination of σ and ζ, our proposed scheme must seem of interest only if it yields significant improvements over the conventional approach in [5] upon implementation in a hybrid model scheme.

The model scheme as presented applies to a fully coherent precipitate with compositionally abrupt interfaces. While main hardening precipitates in age hardenable alloys tend to be highly coherent, they are not always fully coherent. In particular, plate precipitates, of significant importance in e.g. Al–Mg–Si–Cu [29] and Al–Li–Cu [8], almost certainly are incoherent with the host normal to the plate (i.e., along the smallest precipitate dimension). This potentially introduces a subtle problem when recalling the model supercell construction scheme of Fig. 3c: in general, the two halves of the supercell are not intended to represent local regions on the interface separated by the smallest possible distance for the actual precipitate. However, if the precipitate is 'sufficiently small' along merely one dimension, these cell halves will ultimately physically connect across the precipitate, whereby the two local regions described will always be at minimum separation. When this happens, the model scheme evidently breaks down, describing merely the effect of a shear strain on the *whole* precipitate. It follows that plate precipitates must be viewed as impossible to model satisfactorily with the scheme, unless perhaps the plate thickness is sufficiently large (and (12) remains obeyed). In general, as discussed above, problems arise when one or more precipitate dimensions are comparable to the supercell dimensions. This also implies that even fully coherent precipitates can only be reasonably described with the scheme if they have attained a certain size.

Some of the problems of the conventional *ab initio* based interface model scheme of e.g. [9] are retained in the present scheme: interfaces of different orientation do not interact (structurally or electronically), with in particular the description of the precipitate corners hence being dissatisfactory. Further, the interfaces are assumed perfect, i.e., the presence of misfit dislocations is

neglected, even though the presence of such dislocations is well established for large precipitates. These are all topics that would be highly desirable to improve, if possible.

Finally, the calculations on β"/Al have implicitly assumed that compositional disorder is suppressed for the precipitate. This is essentially a computational simplification, questioned experimentally for β" in the literature [30,11]. A potentially more realistic approximation to the physical system would approximate the disorder as e.g. a sequence of alternating β" cells of two different compositions along the precipitate main growth direction. Compositional disorder in the host lattice part of the supercell, i.e., a compositionally diffuse interface, could in principle be investigated in a similar manner, but only within the constraints of a stoichiometric precipitate, as (5), (6), (8), (9) would break down otherwise.

6. Conclusions

We have presented a scheme for DFT based determination of the interfacial and strain energies for an entire fully coherent precipitate-host lattice interface. The basic ingredients of and justifications for the scheme have been outlined, in the simple approximation of zero strain field outside the model region. As a test case we have used the main hardening needle-like precipitate β" of the Al–Mg–Si alloy system, focusing only on a cross section of the full system containing the two highly mismatched interfaces. Largely based on the model scheme structural constraints, we preferred the $Mg_5Al_2Si_4$ composition suggested by Hasting *et al.* in [11] over the alternative Mg_5Si_6 composition. A stoichiometric precipitate with equivalent interface configurations for interfaces of the same orientation was modeled. We find that the strain energies vary almost parabolically along the interfaces, whereas the interfacial energies display clear asymmetric variations. A large part of the strain and interfacial energy asymmetries around the interface center are found to cancel out. Comparison has been made with results obtained within a conventional model scheme, where the same strain field boundary conditions were used. While errors in the LET based determination of the strain energy evolution were highlighted here, we have been unable to draw decisive conclusions on the level of comparability for the two schemes. Our analysis indicates that this question may be significantly affected by the choice of structural boundary condition to the remaining parts of the β"/Al system.

Acknowledgments

This work has been financially supported by the Research Council of Norway via the MultiModAl project (project no. 205353). Simulations were performed through access to the NOTUR facilities. The authors would like to thank J. Friis, SINTEF Materials and Chemistry, for useful comments on the presentation.

Appendix A. Interface region cell geometries and energies

This appendix provides the structural details and calculated energies for the various β"–$Mg_5Al_2Si_4$/Al interface region supercells investigated in this work – commenting also on the associated Al and β" cells used for the separation of the interface energy into interfacial and strain energy contributions. The β"/Al supercell basis vectors for the fully optimized cells describing the **ab** and **cb** interface centers, respectively, are given, in Cartesian coordinates and with unit lengths of 4.05 Å, as: $\mathbf{a}_0^{\mathbf{ab}}$ = (1.5153, 0.4945, –1.0743); $\mathbf{b}_0^{\mathbf{ab}}$ = (0.0000, 0.9891, 0.0000); $\mathbf{c}_0^{\mathbf{ab}}$ = (2.2408, 0.0000, 6.1764); $\mathbf{a}_0^{\mathbf{cb}}$ = (6.1377, 2.0045, –4.1083); $\mathbf{b}_0^{\mathbf{cb}}$ = (0.0000, 0.9996, 0.0000); $\mathbf{c}_0^{\mathbf{cb}}$ = (0.5121, 0.0000, 1.5521). In Table 2, where the cell dimensions of these systems have been included, the value of $|\mathbf{a}_0^{ij}|$ refers to $|2\mathbf{a}_0^{ij} - \mathbf{b}_0^{ij}|$ (conventional cell conversion), for easier comparison with experimental values (see Sec. 4.1 for details).

Table A1. Calculated variation of the β"–$Mg_5Al_2Si_4$/Al $(130)_{Al}$ (**cb**) interface region supercell basis vector $\mathbf{a}_j^{\mathbf{cb}}$ with the position on the interface. The set of vectors are specified in Cartesian coordinates and with unit lengths of 4.05 Å. The calculated interface energies for these systems are also displayed.

Pos. on interface, *j*	$\mathbf{a}_j^{\mathbf{cb}}$	Interface energy (kJ/mol at.)
–1.954	(6.0165, 2.0045, –4.4759)	2.0426
–1.466	(6.0468, 2.0045, –4.3840)	1.8744
–0.977	(6.0771, 2.0045, –4.2921)	1.7593
–0.489	(6.1074, 2.0045, –4.2002)	1.6878
0.000	(6.1377, 2.0045, –4.1083)	1.6624
0.489	(6.1680, 2.0045, –4.0164)	1.6918
0.977	(6.1983, 2.0045, –3.9245)	1.7823
1.466	(6.2286, 2.0045, –3.8326)	1.9347
1.954	(6.2589, 2.0045, –3.7407)	2.1432

Upon cell distortion (modeling of the movement on the interface), $\mathbf{c}_0^{\mathbf{ab}}$ and $\mathbf{a}_0^{\mathbf{cb}}$ were altered as described with (13), (14), while the remaining basis vectors were kept fixed for simplicity. The precipitate-host lattice misfit values employed in this procedure were derived from (19). The resulting basis vectors $\mathbf{c}_i^{\mathbf{ab}}$ and $\mathbf{a}_j^{\mathbf{cb}}$, where *i* and *j* denote the position on the interface in question, are displayed in Table A1, A2, respectively. These tables also comprise the computed interface energies $E^{\mathbf{ab}}_{\text{Int, new, } i}$, $E^{\mathbf{cb}}_{\text{Int, new, } j}$ for this set of cells.

Table A2. Calculated variation of the β"–$Mg_5Al_2Si_4$/Al $(–320)_{Al}$ (**ab**) interface region supercell basis vector $\mathbf{c}_i^{\mathbf{ab}}$ with the position on the interface. The set of vectors are specified in Cartesian coordinates and with unit lengths of 4.05 Å. The calculated interface energies for these systems are also displayed.

Pos. on interface, *i*	$\mathbf{c}_j^{\mathbf{ab}}$	Interface energy (kJ/mol at.)
–1.965	(1.9486, 0.0000, 6.3836)	1.6034
–1.474	(2.0217, 0.0000, 6.3318)	1.4278
–0.982	(2.0947, 0.0000, 6.2800)	1.2993
–0.491	(2.1678, 0.0000, 6.2282)	1.2230
0.000	(2.2408, 0.0000, 6.1764)	1.2020
0.491	(2.3139, 0.0000, 6.1246)	1.2285
0.982	(2.3869, 0.0000, 6.0728)	1.3048
1.474	(2.4600, 0.0000, 6.0210)	1.4280
1.965	(2.5330, 0.0000, 5.9692)	1.5960

The equations linking the information of Table A1, A2 with the local interfacial and strain energy contributions for the **ab** and **cb** interfaces are (5), (8) and (6), (9), respectively. In the present work, we adopted the simplification $\alpha_i^{\mathbf{ab}} = \alpha_0^{\mathbf{ab}}$, $\beta_i^{\mathbf{ab}} = \beta_0^{\mathbf{ab}}$, modifying correspondingly the **cb** interface parameters $\alpha_j^{\mathbf{cb}}$, $\beta_j^{\mathbf{cb}}$. Optimizations of isolated Al and β" cells under the appropriate constraints yielded: $\alpha_0^{\mathbf{ab}} = 0.2590$; $\beta_0^{\mathbf{ab}} = 0.2381$; $\alpha_0^{\mathbf{cb}} = 0.2589$; $\beta_0^{\mathbf{cb}} = 0.2404$. The calculated strain energies (individual Al and β" contributions, see Sec. 5.5 for further comments) have been included in Table A3, A4. The strain energies $\zeta_i^{\mathbf{ab}}$, $\zeta_j^{\mathbf{cb}}$ are given as an average over the two subsystem contributions, since the interface supercell contains an equal amount of precipitate and host lattice atoms.

Table A3. Calculated contributions to the strain energies $\zeta_j^{\mathbf{cb}}$ from the individual β"–$Mg_5Al_2Si_4$ and Al cells (see (10)) as a function of the position on the $(130)_{Al}$ (**cb**) interface.

Pos. on interface, j	$\zeta_j^{\mathbf{cb}}$, β" (kJ/mol at.)	$\zeta_j^{\mathbf{cb}}$, Al (kJ/mol at.)
–1.954	1.1050	0.6543
–1.466	0.8007	0.5411
–0.977	0.5683	0.4692
–0.489	0.4096	0.4403
0.000	0.3280	0.4552
0.489	0.3236	0.5148
0.977	0.3955	0.6157
1.466	0.5429	0.7569
1.954	0.7639	0.9437

Table A4. Calculated contributions to the strain energies $\zeta_i^{\mathbf{ab}}$ from the individual β"–$Mg_5Al_2Si_4$ and Al cells (see (9)) as a function of the position on the $(–320)_{Al}$ (**ab**) interface.

Pos. on interface, i	$\zeta_i^{\mathbf{ab}}$, β" (kJ/mol at.)	$\zeta_i^{\mathbf{ab}}$, Al (kJ/mol at.)
–1.965	0.8112	0.5648
–1.474	0.6051	0.4297
–0.982	0.4517	0.3429
–0.491	0.3587	0.3008
0.000	0.3298	0.2999
0.491	0.3675	0.3429
0.982	0.4727	0.4394
1.474	0.6481	0.5859
1.965	0.8937	0.7779

References

[1] I. J. Polmear, Mater. Forum 28, 1 (2004).

[2] K. Kelton and A. L. Greer, Nucleation in Condensed Matter: Applications in Materials and

Biology, Pergamon (2010), ISBN: 0080421474, p. 538.
[3] E. Hornbogen and E.A. Starke Jr., Acta Metall. Mater., 41, 1 (1993).
[4] Y. Mishin, M. Asta and Ju Li, Acta Mater. 58, 1117 (2010).
[5] V. Vaithyanathan, C. Wolverton and L.-Q. Chen, Phys. Rev. Lett. 88, 125503 (2002).
[6] H. W. Zandbergen, S. J. Andersen and J. Jansen, Science 277, 1221 (1997).
[7] L. Kovarik, S. A. Court, H. L. Fraser and M. J. Mills, Acta Mater. 56, 4804 (2008).
[8] C. Dwyer, M. Weyland, L. Y. Chang and B. C. Muddle, Appl. Phys. Lett. 98, 201909 (2011).
[9] Y. Wang, Z.-K. Liu, L.-Q. Chen and C. Wolverton, Acta Mater. 55, 5934 (2007).
[10] V. Ozolins, C. Wolverton, and A. Zunger, Phys. Rev. B 57, 4816 (1998).
[11] H. S. Hasting, A. G. Frøseth, S. J. Andersen, R. Vissers, J. C. Walmsley, C. D. Marioara, F. Danoix, W. Lefebvre, and R. Holmestad, J. Appl. Phys. 106, 123527 (2009).
[12] We assume here without proof that the point of minimal strain on each interface corresponds to the physical center of this interface. For cases (if any) where this would not hold true, the sums over *i*, *j* in (3) should no longer be symmetric around 0, but the expression would be otherwise unaffected.
[13] Strictly speaking, for the distorted cells, these total energies are approximations to the enthalpies needed in (1).
[14] N. Bernstein, J. R. Kermode, and G. Csanyi, Rep. Prog. Phys. 72, 026501 (2009).
[15] If this should not be the case, the orientation for the interface in question must still hold a well-defined relation (with small near-integer coefficients, as a consequence of the assumed coherency) to the bulk precipitate basis vectors. For this case, it is possible to define a precipitate supercell, replacing the precipitate unit cell in (9) and with the interface running along the new supercell basis vectors.
[16] G. A. Edwards, K. Stiller, G. L. Dunlop, Appl. Surf. Sci. 76/77, 219 (1994).
[17] C. D. Marioara, S. J. Andersen, J. Jansen, and H. W. Zandbergen, Acta Mater. 51, 789 (2003).
[18] S. J. Andersen, H. W. Zandbergen, J. Jansen, C. Træholt, U. Tundal, and O. Reiso, Acta Mater. 46, 3283 (1998).
[19] C. Kittel, Introduction to Solid State Physics, 8th Ed., Wiley (2005), ISBN: 0-471-41526-X, p. 77.
[20] In other words, $e_1 = e_{xx}$; $e_2 = e_{yy}$; $e_3 = e_{zz}$; $e_4 = e_{yz}$; $e_5 = e_{zx}$; $e_6 = e_{xy}$.
[21] P. Hohenberg and W. Kohn, Phys. Rev. 136 B864 (1964).
[22] W. Kohn and L. J. Sham, Phys. Rev. 140 A1133 (1965).

[23] D. Vanderbilt, Phys. Rev. B 32, 8412 (1985).
[24] G. Kresse and J. Hafner, Phys. Rev. B 47 R558 (1993).
[25] G. Kresse and J. Furthmüller, Comput. Mater. Sci. 6, 15 (1996).
[26] J. P. Perdew, J. A. Chevary, S. H. Vosko, K. A. Jackson, M. R. Pederson, D. J. Singh, and C. Fiolhais, Phys. Rev. B 46, 6671 (1992).
[27] A. E. Mattsson, P. A. Schultz, M. P. Desjarlais, T. R. Mattsson, and K. Leung, Model. Simul. Mater. Sci. Eng. 13, R1 (2005).
[28] C. D. Marioara, S. J. Andersen, H. W. Zandbergen, and R. Holmestad, Metall Mater Trans A 36A, 691 (2005).
[29] C. D. Marioara, S. J. Andersen, T. N. Stene, H. Hasting, J. Walmsley, A. T. J. van Helvoort and R. Holmestad, Philos. Mag. 87, 3385 (2007).
[30] M. A. van Huis, J. H. Chen, H. W. Zandbergen and M. H. F. Sluiter, Acta Mater. 54, 2945 (2006).